Sādhanā (2021)46:1
https://doi.org/10.1007/s12046-020-01523-x

© Indian Academy of Sciences

Optimal low-thrust GTO–GSO transfers using differential evolution

PADMANABHA PRASANNA SIMHA[1,*] and R V RAMANAN[2]

[1] Vikram Sarabhai Space Centre, Thiruvananthapuram, India
[2] Indian Institute of Space Science and Technology, Thiruvananthapuram, India
e-mail: padmanabhapsimha@gmail.com; padmanabha_prasanna@vssc.gov.in; rvramanan@iist.ac.in

MS received 21 February 2019; revised 12 May 2020; accepted 5 October 2020

Abstract. Transfers from geosynchronous transfer orbits (GTO) to geosynchronous orbits (GSO) using electric propulsion have been optimized in the current study. Both time-optimal and fuel-optimal trajectories are generated. Three-dimensional equations of motion are considered for the system dynamics. The indirect approach based on optimal control theory is followed and the resulting two-point boundary value problem is solved using differential evolution, a search-based global optimization technique. Optimal trajectories for various mission scenarios are obtained using differential evolution and compared to transfers presented in literature.

Keywords. Low thrust; trajectory optimization; differential evolution.

1. Introduction

Launch vehicle upper stages usually deploy satellites into a geosynchronous transfer orbit (GTO) from which the final geostationary orbit (GSO) is achieved by means of the propulsion system of the spacecraft. This transfer involves both orbital size change as well as plane change manoeuvres. Using conventional high-thrust chemical propulsion systems, the spacecraft performs a series of orbit raising manoeuvres combined with plane change manoeuvres to enter into a 24-hour equatorial orbit. Low-thrust spacecraft need to thrust for several months to be able to raise themselves to their required altitude and plane change. Optimizing these transfers can help in saving propellant mass, increasing the payload to GSO. This increases the operational life of the satellites due to the higher specific impulse achievable by low-thrust electric propulsion systems.

In Ref. [1] the problem of fuel-optimal GTO–GSO transfer has been solved by assuming a certain thrust–coast control profile. The thrust arc angles are fixed at the apogee of the GTO. Parametric studies on the effect of this arc length have been performed. It is found that results from the current fuel-optimal control law significantly deviate from this assumption. Compared with the formulation in Ref. [1], the current approach has no singularities in the formulation and can handle cases with zero eccentricity. In Ref. [2], GTO–GSO time-optimal transfer problems have been solved by the direct approach to optimization method using collocation. In general, gradient optimization techniques are used. This leads to requirements for accurate initial guesses for the trajectories and control profiles. In Ref. [3], the authors compare guidance laws to optimal control results. It is found that the current formulation is capable of giving better optimal solutions for the time-optimal fuel fraction and flight duration. In Ref. [4], the complete fuel-optimal control problem is solved with no assumptions on the thrust–coast control profile. However, the computational time is very high in this formulation due to the use of homotopy methods. The current formulation does not require any numerical continuation techniques like homotopy due to the insensitivity of the differential evolution (DE) algorithm to the initial guess (or bounds on the initial costate values).

2. Mathematical formulation

The Earth Centred Inertial (ECI) frame has been utilized for all the computations in this study. Cartesian coordinates have been used.

2.1 *Problem geometry*

As illustrated in figure 1, the spacecraft is placed into an initial GTO by the launch vehicle. Using available onboard electric propulsion systems, the spacecraft has to raise itself to the final GSO orbit. This requires increasing the semi-major axis while bringing the eccentricity and the orbital inclination to zero.

---

*For correspondence

Published online: 01 February 2021

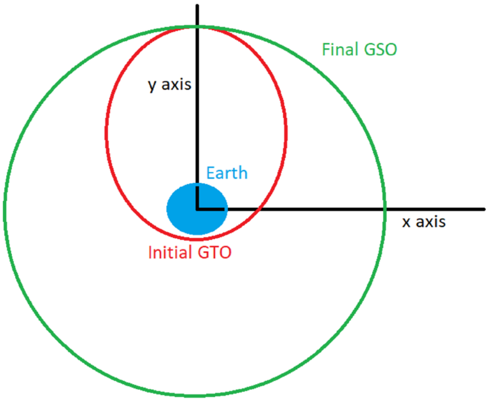

Figure 1. 2D projection of the GTO–GSO transfers considered in this study.

2.2 *State equations*

The following equations govern the dynamics in terms of the state of the system $[x\ y\ z\ v_x\ v_y\ v_z\ m]$ and the controls $[\alpha_x\ \alpha_y\ \alpha_z]$, which are components of the acceleration vector due to thrust:

$$\dot{x} = v_x, \tag{1}$$

$$\dot{y} = v_y, \tag{2}$$

$$\dot{z} = v_z \tag{3}$$

$$\dot{v}_x = -\mu_p \frac{x}{r^3} + \mu_s\left[-\frac{x_s}{r_s^3} - \frac{x - x_s}{(r - r_s)^3}\right] + \alpha_x, \tag{4}$$

$$\dot{v}_y = -\mu_p \frac{y}{r^3} + \mu_s\left[-\frac{y_s}{r_s^3} - \frac{y - y_s}{(r - r_s)^3}\right] + \alpha_y, \tag{5}$$

$$\dot{v}_z = -\mu_p \frac{z}{r^3} + \mu_s\left[-\frac{z_s}{r_s^3} - \frac{z - z_s}{(r - r_s)^3}\right] + \alpha_z, \tag{6}$$

$$\dot{m} = -\frac{m}{g_0 I_{sp}}\sqrt{\alpha_x^2 + \alpha_y^2 + \alpha_z^2}. \tag{7}$$

These equations assume spacecraft motion in an inertial frame under the action of a spherical central body, a single third body perturbing force and the accelerations due to the thrust. The effect of lunar perturbations can be included by adding the gravitational parameter of the Moon (μ_m) in a similar manner. If only the Earth's gravity (spherical) is to be considered, then μ_s or μ_m can be taken as zero.

2.3 *Cost function and control constraints*

In order to optimize the trajectory, a cost function has to be minimized. We consider the problems of time-optimal and fuel-optimal transfers.

For time-optimal transfers, the transfer duration is to be minimized. The cost function can be written as follows:

$$J_{time} = \Phi_f + \int_{t_0}^{t_f} dt. \tag{8}$$

The optimization variables for the time-optimal problem are the costate variables λ_x, λ_y, λ_z, λ_{v_x}, λ_{v_y}, λ_{v_z}, λ_m and the time of flight t_f.

For fuel-optimal transfers, the transfer duration is set to a value greater than or equal to the time duration of the time-optimal transfer. The following cost function is formulated:

$$J_{fuel} = \Phi_f + \int_{t_0}^{t_f} \frac{m}{g_0 I_{sp}}\sqrt{\alpha_x^2 + \alpha_y^2 + \alpha_z^2}dt. \tag{9}$$

The optimization variables for the fuel-optimal problem are the costate variables λ_x, λ_y, λ_z, λ_{v_x}, λ_{v_y}, λ_{v_z} and λ_m. The time of flight has to be fixed to a value greater than or equal to the minimum flight duration obtained from the time-optimal formulation.

In equations (8) and (9), Φ_f represents the error in achieving the final orbit. It has to be driven down to zero in order to ensure accurate orbit insertion. The second term containing the integral represents either the transfer duration or the propellant expenditure over the whole trajectory and is to be minimized.

$$\Phi_f = |1 - \frac{a_{actual}}{a_{desired}}|^2 + |\hat{h}_{actual} - \hat{h}_{desired}|^2 + |\vec{\mathbf{e}}_{actual} - \vec{\mathbf{e}}_{desired}|^2. \tag{10}$$

Here, a is the two-body semi-major axis, $\hat{h}$ is the unit angular momentum vector and $\mathbf{e}$ is the eccentricity vector. They can be computed from the state vector by standard two-body relations. This function is minimized using DE. The second (integral) term of the cost functions is optimized using Pontryagin's minimum principle [5].

2.4 *Control constraints*

In order to model the limitations of the thruster, the following constraint is introduced:

$$m\sqrt{\alpha_x^2 + \alpha_y^2 + \alpha_z^2} \le T_{max}. \tag{11}$$

2.5 *TPBVP formulation*

Corresponding to the states $[x\ y\ z\ v_x\ v_y\ v_z\ m]$, costates $[\lambda_x\ \lambda_y\ \lambda_z\ \lambda_{v_x}\ \lambda_{v_y}\ \lambda_{v_z}\ \lambda_m]$ are introduced. The Hamiltonians for the time-optimal ($\boldsymbol{H}'_{time}$) and fuel-optimal problems ($\boldsymbol{H}'_{time}$) are expressed as follows:

$$
\begin{aligned}
\boldsymbol{H}'_{\boldsymbol{time}} = {} & 1 - \lambda_m\left(\frac{m\sqrt{\alpha_x^2+\alpha_y^2+\alpha_z^2}}{g_0 I_{sp}}\right) + \lambda_x v_x + \lambda_y v_y + \lambda_z v_z \\
& + \lambda_{v_x}\left[-\frac{\mu_p x}{r^3} - \mu_s\left(\frac{x_s}{r_s^3} + \frac{x - x_s}{(r - r_s)^3}\right) + \alpha_x\right] \\
& + \lambda_{v_y}\left[-\frac{\mu_p y}{r^3} - \mu_s\left(\frac{y_s}{r_s^3} + \frac{y - y_s}{(r - r_s)^3}\right) + \alpha_y\right] \\
& + \lambda_{v_z}\left[-\frac{\mu_p z}{r^3} - \mu_s\left(\frac{z_s}{r_s^3} + \frac{z - z_s}{(r - r_s)^3}\right) + \alpha_z\right],
\end{aligned}
\tag{12}
$$

$$
\begin{aligned}
\boldsymbol{H}'_{\boldsymbol{fuel}} = {} & (1 - \lambda_m)\left(\frac{m\sqrt{\alpha_x^2+\alpha_y^2+\alpha_z^2}}{g_0 I_{sp}}\right) + \lambda_x v_x + \lambda_y v_y + \lambda_z v_z \\
& + \lambda_{v_x}\left[-\frac{\mu_p x}{r^3} - \mu_s\left(\frac{x_s}{r_s^3} + \frac{x - x_s}{(r - r_s)^3}\right) + \alpha_x\right] \\
& + \lambda_{v_y}\left[-\frac{\mu_p y}{r^3} - \mu_s\left(\frac{y_s}{r_s^3} + \frac{y - y_s}{(r - r_s)^3}\right) + \alpha_y\right] \\
& + \lambda_{v_z}\left[-\frac{\mu_p z}{r^3} - \mu_s\left(\frac{z_s}{r_s^3} + \frac{z - z_s}{(r - r_s)^3}\right) + \alpha_z\right].
\end{aligned}
\tag{13}
$$

These Hamiltonians are used to derive the costate dynamics by taking partial of the Hamiltonian with the respective state variables:

$$
\dot{\bar{\lambda}} = \frac{\partial \boldsymbol{H}}{\partial \bar{x}}. \tag{14}
$$

The optimal control law is determined by applying Pontryagin's minimum principle subject to the constraints on the control. Since there are constraints on both time- and fuel-optimal problems, Pontryagin's minimum principle has to be applied to the augmented Hamiltonians by either the Karush–Kuhn–Tucker (KKT) conditions or by the classical Lagrange multiplier technique based on the nature of the constraint. The augmented Hamiltonians are as follows:

$$
\boldsymbol{H}_{\boldsymbol{time}} = \boldsymbol{H}'_{\boldsymbol{time}} + \eta\left[m\sqrt{a_x^2+a_y^2+a_z^2} - T_{max}\right], \tag{15}
$$

$$
\boldsymbol{H}_{\boldsymbol{fuel}} = \boldsymbol{H}'_{\boldsymbol{fuel}} + l\left[m\sqrt{a_x^2+a_y^2+a_z^2} - T_{max}\right]. \tag{16}
$$

Here, η is the Lagrange multiplier for the equality constraint and l is the multiplier that arises from the KKT conditions for constrained minimization with inequality constraints.

2.6 *Costate dynamics*

For brevity, only the fuel-optimal costate equations are presented here. The time-optimal costate equations can be similarly derived.

$$
\begin{aligned}
\dot{\lambda}_x = -\frac{\partial \boldsymbol{H}_{\boldsymbol{fuel}}}{\partial x} = {} & -\lambda_{v_x}\left[\psi + 3\frac{x}{r}\epsilon_x\right] \\
& - \lambda_{v_y}\left[3\frac{x}{r}\epsilon_y\right] - \lambda_{v_z}\left[3\frac{x}{r}\epsilon_z\right]
\end{aligned}
\tag{17}
$$

$$
\begin{aligned}
\dot{\lambda}_y = -\frac{\partial \boldsymbol{H}_{\boldsymbol{fuel}}}{\partial y} = {} & -\lambda_{v_x}\left[3\frac{y}{r}\epsilon_x\right] - \lambda_{v_y}\left[\psi + 3\frac{y}{r}\epsilon_y\right] \\
& - \lambda_{v_z}\left[3\frac{y}{r}\epsilon_z\right]
\end{aligned}
\tag{18}
$$

$$
\begin{aligned}
\dot{\lambda}_z = -\frac{\partial \boldsymbol{H}_{\boldsymbol{fuel}}}{\partial z} = {} & -\lambda_{v_x}\left[3\frac{z}{r}\epsilon_x\right] - \lambda_{v_y}\left[3\frac{z}{r}\epsilon_y\right] \\
& - \lambda_{v_z}\left[\psi + 3\frac{z}{r}\epsilon_z\right]
\end{aligned}
\tag{19}
$$

$$
\dot{\lambda}_{v_x} = -\frac{\partial \boldsymbol{H}_{\boldsymbol{fuel}}}{\partial v_x} = -\lambda_x \tag{20}
$$

$$
\dot{\lambda}_{v_y} = -\frac{\partial \boldsymbol{H}_{\boldsymbol{fuel}}}{\partial v_y} = -\lambda_y \tag{21}
$$

$$
\dot{\lambda}_{v_z} = -\frac{\partial \boldsymbol{H}_{\boldsymbol{fuel}}}{\partial v_z} = -\lambda_z \tag{22}
$$

$$
\dot{\lambda}_m = -\frac{\partial \boldsymbol{H}_{\boldsymbol{fuel}}}{\partial m} = -\frac{(1 - \lambda_m)\sqrt{\alpha_x^2+\alpha_y^2+\alpha_z^2}}{g_0 I_{sp}} \tag{23}
$$

where

$$
\psi = -\frac{\mu_p}{r^3} - \frac{\mu_s}{(r - r_s)^3} \tag{24}
$$

$$
\epsilon_x = \frac{\mu_p x}{r^4} + \frac{\mu_s(x - x_s)}{(r - r_s)^4} \tag{25}
$$

$$
\epsilon_y = \frac{\mu_p y}{r^4} + \frac{\mu_s(y - y_s)}{(r - r_s)^4} \tag{26}
$$

$$
\epsilon_z = \frac{\mu_p z}{r^4} + \frac{\mu_s(z - z_s)}{(r - r_s)^4}. \tag{27}
$$

This system of differential equations require x_s, y_s, z_s and r_s as a function of time. They can be obtained either from standard ephemeris data or by series expansions.

The time-optimal costate equations are almost the same except for the costate equation for spacecraft mass. The modified time-optimal costate equation for mass is shown in equation (28):

$$
\dot{\lambda}_m = -\frac{\partial \boldsymbol{H}_{\boldsymbol{time}}}{\partial m} = -\frac{\lambda_m\sqrt{\alpha_x^2+\alpha_y^2+\alpha_z^2}}{g_0 I_{sp}}. \tag{28}
$$

From the state and fuel-optimal costate dynamics, the following conserved quantity is obtained:

$$m(1 - \lambda_m) = Q. \tag{29}$$

Here, Q is a conserved quantity along the optimal trajectory. This can be used to reduce the number of differential equations from 14 to 13.

From the state and time-optimal costate dynamics, the following identity can be derived:

$$\dot{m}\lambda_m = \dot{\lambda_m} m. \tag{30}$$

This identity can be used to eliminate the differential equation for λ_m from the costate dynamics and replace it with an analytical expression as follows,

$$\lambda_m(t_2) = K\lambda_m(t_1)\frac{m(t_2)}{m(t_1)}. \tag{31}$$

Here K is an arbitrary constant. This helps in decreasing computational time as the number of equations to be numerically integrated in three dimensions drops from 14 to 13.

Further, as the system is autonomous (no explicit time dependence), the Hamiltonian is also invariant with time for both fuel-optimal and time-optimal problems. This can be used to further reduce the number of differential equations to 12 by choosing the Hamiltonian to be an arbitrary constant. However, this is not used in this study and the full set of equations have been integrated to verify the accuracy of the dynamics.

2.7 *Optimal control law*

Pontryagin's minimum principle is used to derive the optimal control law as a function of the states and costates. Mathematically, it can be stated as follows:

$$\{\alpha_x^*, \alpha_y^*, \alpha_z^*\} = argmin\{\boldsymbol{H}(\boldsymbol{x}^*, \boldsymbol{\lambda}^*, \boldsymbol{\alpha})\}. \tag{32}$$

Performing this minimization requires the application of the KKT conditions or using Lagrange multipliers. It has also been identified through analysis that intermediate values of thrust are not possible as solutions satisfying the Pontryagin's minimum principle for these types of control constraints and cost functional lead to either zero or maximum available thrust. However, the singular control arcs are ignored.

The following control law is obtained for the fuel-optimal problem:

$$\begin{cases} \text{if } l \geq 0, & \alpha_x^* = k_{max}\lambda_{v_x} \quad \alpha_y^* = k_{max}\lambda_{v_y} \quad \alpha_z^* = k_{max}\lambda_{v_z}, \\ \text{if } l < 0, & \alpha_x^* = k_{min}\lambda_{v_x} \quad \alpha_y^* = k_{min}\lambda_{v_y} \quad \alpha_z^* = k_{min}\lambda_{v_z}, \end{cases} \tag{33}$$

$$l = \frac{\sqrt{\lambda_{v_x}^2 + \lambda_{v_y}^2 + \lambda_{v_z}^2}}{m} - \frac{1 - \lambda_m}{g_0 I_{sp}}, \tag{34}$$

$$k_{max} = -\frac{T_{max}}{m\sqrt{\lambda_{v_x}^2 + \lambda_{v_y}^2 + \lambda_{v_z}^2}}, \tag{35}$$

$$K_{min} = 0. \tag{36}$$

For the time-optimal problem, the control law remains identical except for

$$k_{min} = k_{max} = -\frac{T_{max}}{m\sqrt{\lambda_{v_x}^2 + \lambda_{v_y}^2 + \lambda_{v_z}^2}}. \tag{37}$$

3. Solution methodology

The solution to the resulting TPBVP is reduced to determining the costates at time t_0 such that when the state and costate dynamics are numerically integrated, the final state vector at time t_f lies on the final desired orbit. This is achieved by driving Φ_f to zero. The costates are determined using DE by defining bounds on each costate variable.

For time-optimal problems, the flight duration is also treated as an optimization variable and the flight duration that solves the TPBVP (two-point boundary value problem) is taken as the minimum flight duration. In the case of fuel-optimal problems, the flight duration is fixed to a value greater than or equal to the obtained time-optimal flight duration. When the flight durations for the time-optimal and fuel-optimal formulations are the same, the solutions are identical. For flight durations greater than the time-optimal solution, it is possible that the fuel requirement is lowered. This happens because periods of coasting arise where no fuel is consumed. If the flight duration is set to values below the time-optimal solution, then solutions do not exist.

3.1 *DE*

DE is a search-based global optimization method. It has been shown to be effective in solving complex optimization problems even with badly behaved functions as demonstrated in Ref. [6]. DE has three operations, namely crossover, mutation and selection. Three DE parameters are used to represent and control the DE process. They are the crossover ratio (CR), mutation factor (F) and population size (NP). They are together represented as CR/F/NP. DE involves the construction of an initial random population in a hyper-box of allowed values for the optimization

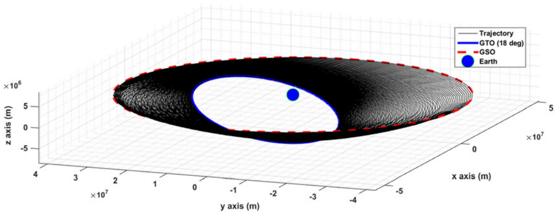

Figure 2. A typical low-thrust GTO–GSO trajectory.

variables. New population members are generated by the operations of crossover and mutation by combining existing members according to certain rules. The new member is made to replace the old one if the cost value of the newer member is lower. This strategy is elitist as the overall minimum cost of the population either remains constant or decreases. This results in rapid convergence. More details on the DE algorithm and variants are available in Ref. [7].

3.2 *Numerical integration*

The state and costate dynamics have to be accurately integrated numerically to obtain the optimal trajectory. In this study, the Runge–Kutta–Fehlberg 7(8) scheme is utilized. It has a high order of accuracy and provides adaptive time stepping [8].

4. Time-optimal transfers

4.1 *Typical trajectory*

For demonstration, a 1000-kg spacecraft with 300 mN of thrust and a specific impulse of 2000 s is transferred from a GTO inclined at 18 degrees to the Earth equator to an equatorial GSO. This GTO inclination corresponds to the one achievable from SDSC-SHAR (Satish Dhawan Space Center – Sriharikota High Altitude Range). The GTO is a 250 km × 35768 km orbit and the GSO is a 35768-km circular orbit. The optimal trajectory is plotted in figure 2.

The inclination and eccentricity have to be driven down to zero as the final GSO is a circular orbit. Figures 3 and 4 show, respectively, the inclination and eccentricity profiles. It is seen that they gradually drop to zero. For this transfer the total propellant mass utilized is 118.9 kg with the spacecraft initial mass at 1000 kg.

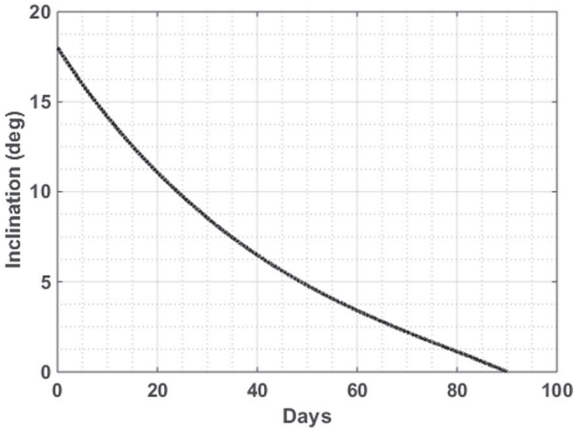

Figure 3. A typical GTO–GSO transfer inclination profile.

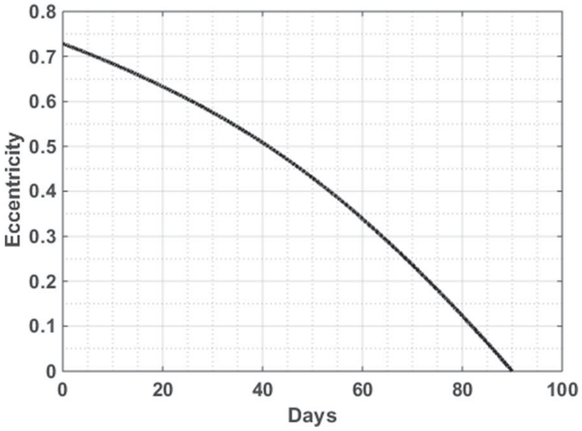

Figure 4. A typical GTO–GSO transfer eccentricity profile.

4.2 *Influence of launch site latitude*

The launch site latitude plays an important role in the transfer as it governs the minimum inclination of the GTO that can be delivered by the launch vehicle. A satellite equipped with a high-thrust hypergolic bipropellant system with specific impulse of 315 s would require a propellant mass fraction of 0.4096 if a single combined orbit raising and plane change manoeuvre is done at the apogee of the GTO with 18 degrees inclination (assuming that the apogee of the GTO lies on the GSO orbit). The same transfer using electric propulsion systems with a specific impulse of 2000 s requires a propellant fraction of only 0.1189 at the expense of long flight duration. This highlights the huge benefits that electric propulsion offers in performing GTO–GSO orbit transfers. Further, it is seen from figure 5 that even from very high latitudes such as the Plesetsk Cosmodrome, the propellant fraction with electric propulsion requires only 0.1829 as the propellant fraction as seen in figure 5. To perform the same with chemical systems would require a fraction of 0.617, which could render this infeasible.

4.3 *Influence of thrust level*

The thrust level plays a huge role in these transfers as it significantly affects the flight duration. Figure 6 shows that

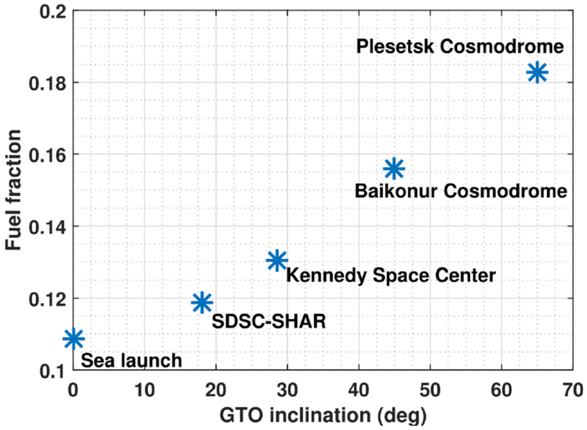

Figure 5. Influence of launch site latitude (GTO inclination).

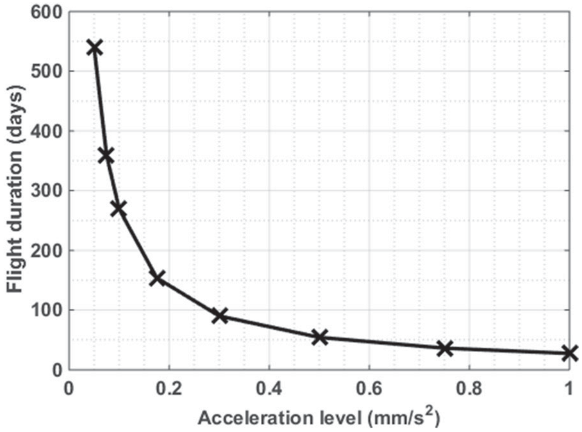

Figure 6. Flight duration vs initial acceleration.

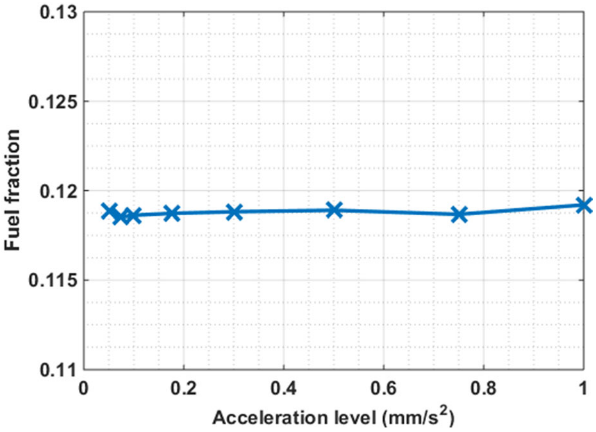

Figure 7. Fuel fraction vs initial acceleration.

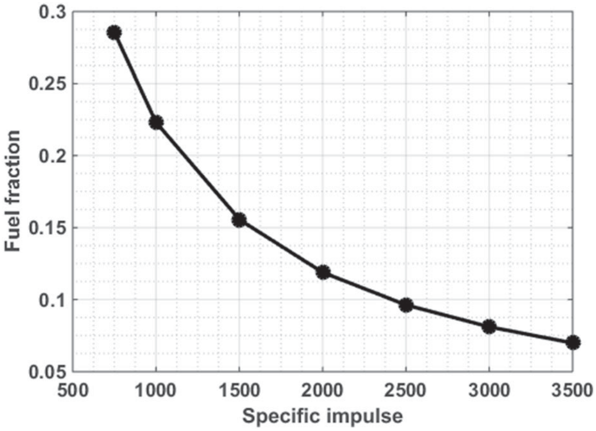

Figure 8. Influence of specific impulse on fuel fraction.

for very low values of initial acceleration, the flight duration shoots up as the spacecraft has to execute a huge number of spirals around the Earth in order to perform the orbit raising and plane change. These results are obtained for the same GTO as in the previous case with a spacecraft of initial mass 1000 kg and thruster specific impulse of 2000 s.

Figure 7 shows that the propellant fraction (propellant mass required to initial spacecraft mass ratio) changes marginally ($<$0.07%) for even large changes in acceleration levels. This suggests that the manoeuvre efficiency is roughly the same irrespective of the acceleration level in very-low-thrust transfers. This is in contrast with high-thrust manoeuvres, which can suffer from significant degradation in propellant fractions due to finite burn losses.

These time-optimal results show that low-thrust propulsion systems can offer significant benefits in terms of payload mass delivered to GSO. However there can be concerns regarding radiation levels and radiation hardening requirement as the spacecraft will have to enter and exit the inner van Allen radiation belt multiple times. These concerns are not addressed in this study.

4.4 *Influence of specific impulse*

Figures 8 and 9 depict the variation of propellant fraction and flight duration with variation in the thruster specific impulse keeping all other parameters constant. It is seen that there is significant change in the propellant mass required but the change in flight duration is low.

It is observed that even for low specific impulses of about 750 s, the fuel fraction is lower than 30%. This is significantly better than those of chemical propulsion systems. In some cases it may be of greater advantage to utilize lower specific impulse thrusters as they consume lesser electrical power for the same thrust produced compared with higher specific impulse thrusters at the same thrust level. This depends on the mission requirements and the specific impulse and thrust levels need to be tailored accordingly.

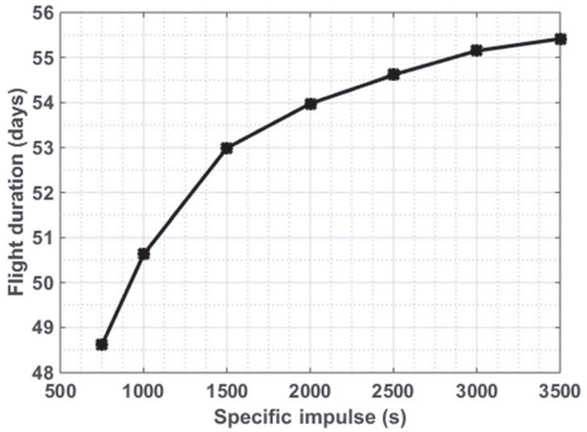

Figure 9. Impact of specific impulse on flight duration.

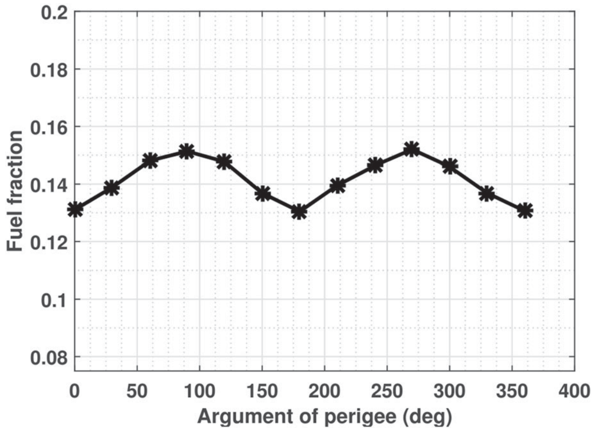

Figure 10. Influence of GTO argument of perigee on fuel fraction.

4.5 *Influence of GTO argument of perigee*

Figure 10 shows the variation of the fuel fraction with changes in the orbit's argument of perigee. The spacecraft is the same as taken in the previous cases with the exception that the initial GTO is delivered by a launch from the Kennedy Space Center with an inclination of 28.5 degrees. It is seen that even large changes in the argument of perigee amount to roughly only a 2% penalty in the fuel fraction with the maximum occurring when the perigee or apogee is oriented 90 degrees to the nodal line.

These results show that using low-thrust, high specific impulse propulsion systems, GTO–GSO missions become very flexible in comparison with missions using chemical propulsion systems. All these results have been obtained using the proposed solution methodology, which has been observed to be robust and provides solutions without any requirement for accurate initial solutions.

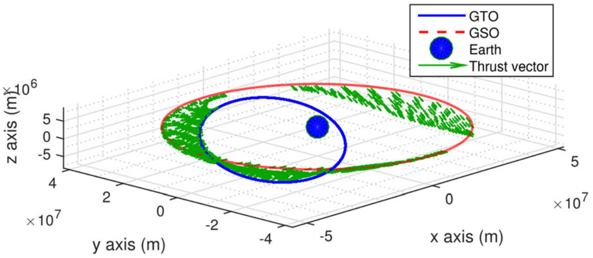

Figure 11. Typical fuel-optimal trajectory. Thrust vectors are shown. Large periods of coasting are visible.

5. Fuel-optimal transfers

This problem is relatively unexplored due to the significant numerical difficulties that are encountered while attempting a solution. The control profile experiences a huge number of switches from thrust to coast and vice versa. However, at the expense of increased flight duration, it is possible to get lower propellant consumption. In Ref. [4], homotopy is used to obtain numerical solutions. The current method is capable of arriving at optimal trajectories without using homotopy or any numerical continuation methods.

Figure 11 shows a typical fuel-optimal trajectory for a flight duration of 112.5 days with 300 mN of thrust and a specific impulse of 2000 s. The regions with the arrows represent the portion of the orbit where the thruster is fired. The rest of the trajectory comprises coasts, which do not require the thruster to be fired. In Ref. [1], the thrust–coast arcs are assumed a priori. The thrusting arcs obtained here are very different. Significantly better optimal results are obtained with the solution of the full fuel-optimal control problem.

Figure 12 shows the complex thrust profile that arises from the fuel-optimal GTO–GSO transfer problem. Obtaining this solution is much more difficult than a time-optimal solution. All these thrust switchings have been resolved by the numerical method without any external input. This demonstrates the capability of DE to handle extremely complex optimization problems.

Flight duration affects the fuel fraction significantly. Increasing the flight duration leads to lower fuel consumption.

Tables 1 and 2 show fuel-optimal results compared with the time-optimal values for the GTO from Kennedy Space Center. It is seen that an appreciable decrease in the propellant fraction can be attained.

For comparison with the strategy of Ref. [1], a 5365 kg spacecraft with 400 mN of thrust is considered. It is seen that the current optimal control strategy is capable of delivering larger payloads for both the continuous thrusting and fuel-optimal frameworks. The results are tabulated in table 3. The fuel-optimal solution also has a vastly different thrust profile compared with what was assumed in [1].

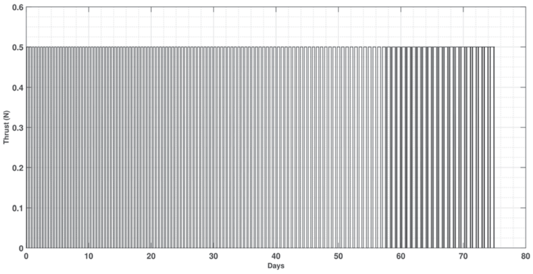

Figure 12. Fuel-optimal trajectory control profile.

Table 1. Fuel-optimal results for 500-mN thrust.

Formulation	Flt. time (days)	Fuel fraction
Time-optimal	59.987	0.13214
Fuel-optimal	67.500	0.11600
Fuel-optimal	70.000	0.11355
Fuel-optimal	75.000	0.10832
Fuel-optimal	80.000	0.10716
Fuel-optimal	85.000	0.10371
Fuel-optimal	90.000	0.10264

Table 2. Fuel-optimal results for 300-mN thrust.

Formulation	Flt. time (days)	Fuel fraction
Time-optimal	099.178	0.13018
Fuel-optimal	112.500	0.11862
Fuel-optimal	125.000	0.10971
Fuel-optimal	137.500	0.10500

Table 3. Comparison of results with Ref. [1].

Formulation	Flt. time (days)	Fuel fraction
Ref. [1]	500.0	0.06710
Current	500.0	0.06296
Ref. [1] (min time)	≈365.0	≈0.09320
Current (min time)	335.9	0.08487

For comparison with results in Refs. [2, 3], a 1200-kg spacecraft with 311.6 mN of thrust at 1800-s specific impulse is considered. The current formulation outperforms the direct optimization techniques used as well as the guidance strategies presented in [2, 3]. The results have been shown in table 4.

6. Solar perturbations

The Sun's effect on the GTO–GSO transfer is shown in table 5. It is seen that the inclusion of the perturbing force in the costate dynamics is essential, else suboptimal results are obtained. The departure epochs are varied in steps of 3 months (300-mN thrust, 2000-s I_{sp} with 1000-kg initial spacecraft mass). Nonetheless, it is seen that the influence of the Sun is minimal on the fuel fraction once properly accounted for. For some epochs the Sun provides a small benefit while for other departure epochs, the Sun can lead to small penalties in the fuel fraction.

Table 4. Comparison with results from and cited in [2, 3].

Solution method	Flt. time (days)	Fuel fraction
Current	114.88	0.14601
Collocation	118.29	0.15035
Kluever	118.36	0.15044
SEPSPOT	118.29	0.15035
DAG	125.60	0.15636
Q-law	120.02	0.14966

Table 5. Influence of solar gravity on GTO–GSO fuel fraction for 500-mN thrust.

Departure date (Julian)	Earth alone	Sun in state dynamics	Sun in state & costate dynamics
2458287.000	0.13214	0.13711	0.13197
2458378.313	0.13214	0.13455	0.13186
2458469.625	0.13214	0.13749	0.13312
2458560.938	0.13214	0.13457	0.13220
2458652.250	0.13214	0.13708	0.13129

Table 6. Influence of lunar gravity on GTO–GSO fuel fraction for 500-mN thrust (time-optimal transfer).

Departure epoch (Julian)	Earth alone	Earth + Moon
2458287.00	0.13214	0.14486
2458294.00	0.13214	0.14915
2458301.00	0.13214	0.14936
2458308.00	0.13214	0.14897
2458315.00	0.13214	0.14619
2458322.00	0.13214	0.14808

Table 7. Influence of lunar gravity on GTO–GSO fuel fraction for 500-mN thrust (75-day fuel-optimal transfer).

Departure epoch (Julian)	Earth alone	Earth +Moon
2458287.00	0.10832	0.10979
2458294.00	0.10832	0.10981
2458301.00	0.10832	0.11104
2458308.00	0.10832	0.11032
2458315.00	0.10832	0.11094
2458322.00	0.10832	0.10920

Table 8. Comparison of the current method with some others from literature.

Method	Singularity	Direct/indirect	Single/multiple shooting	Homotopy	State vector
Current method	None	Indirect	Single	No	Cartesian
Ref. [1]	Yes (at $e = 0$ and at $i = 0$)	Variational equations	NA	NA	Non-Cartesian
Ref. [2]	None	Direct collocation + orbit averaging	NA	No	Non-Cartesian
Ref. [3]	None	NA (guidance laws)	NA	No	Non-Cartesian
Ref. [4]	None	Indirect	Single	Yes	Non-Cartesian

7. Lunar perturbations

It is seen from table 6 that for time-optimal GTO–GSO transfers, lunar perturbations has a much more significant impact with over 1.6% increase in fuel fraction.

For fuel-optimal transfers (table 7), the lunar influence is diminished with the maximum penalty in fuel fraction being less than 0.3%. The departure epochs are varied in steps of 7 days. It is seen that for the whole lunar cycle, perturbations result in a penalty that, in the case of time-optimal transfers, is significant but the effect rapidly diminishes when the flight duration is increased.

8. Comparison with literature

In the case of fuel-optimal trajectories, the fuel fraction required is less at the expense of larger flight durations. Reference [1] has singularities and cannot handle zero inclination or eccentricity orbits. The current approach has no such singularities. It outperforms the direct optimal control results as well as the guidance law strategies given in Refs. [2, 3]. The obtained fuel results are comparable to results from Ref. [4] and the thrust–coast control profile shows the same behaviour with the thrusting occurring at the same spatial locations. The advantage of the current formulation when compared with that followed in Ref. [4] is that numerical continuation methods like homotopy are avoided when DE is applied to solve the resulting TPBVP. The comparisons have been summarized in a tabular form (table 8). Additionally, the method in the current study does not require any initial guess on the trajectory unlike other methods. Most gradient-descent-based methods require good initial guesses even with homotopy in order to converge to a solution. The DE algorithm used here is capable of arriving at the final solution even with wide bounds on the initial costates.

9. Conclusions and future work

The current paper demonstrates results for GTO–GSO transfers in both fuel- and time-optimal frameworks using the indirect approach to optimal control. It is found that for low-thrust transfers, even large deviations in the argument of perigee lead to only about a 2% penalty in the fuel fraction (for 2000-s specific impulse). Time-optimal GTO–GSO transfer fuel fractions are found to be insensitive to the spacecraft's thrust level. For a wide range of flight durations, the propellant consumption remains roughly the same. Higher specific impulses lead to lesser fuel consumption. It is seen that increasing the specific impulse leads to longer travel times as the spacecraft tends to remain more massive due to lower mass consumption even with same thrust levels.

This investigation indicates that DE may be applicable to trajectory optimization problems that are much more difficult. Numerically intractable solutions can now be obtained in reasonable computer time. The other advantage of this method is that it is easily parallelized and the parallelization has been verified up to 8 cores in the current study. The algorithm can also be extended to larger distributed computing systems. There are some issues regarding load imbalance, especially during the initial generations of the DE algorithm run due to the unequal times to which trajectory evolution has to be performed by the different compute nodes. This issue is alleviated naturally as convergence to the optimal solution is under way.

Solar and lunar perturbations on the GTO–GSO transfer have been investigated for a wide range of departure epochs. It is found that the solar influence is very minimal and can either lead to a small benefit or penalty in the time-optimal case. It has been observed that the inclusion of the perturbing dynamics in the costate equations is mandatory. Failing to do so will result in sub-optimal solutions. This suggests that future results including non-spherical earth effects must include the perturbations in both the state and costate equations. Lunar perturbations have been found to be much more severe on the time-optimal trajectories obtained. The penalty in fuel fraction depending on the departure epoch can be over 1.6%. This high value decreases to a maximum of about 0.3% for 75-day fuel-optimal trajectories. The penalty is also found to depend on the departure epoch as expected. This dependence comes about due to changes in the relative geometry of the Earth–Moon system and the spacecraft.

Non-spherical gravity effects can be significant. They can be easily accommodated in the state equations of motion. Incorporating the perturbations analytically into the optimal control formulation and the costate equations is a tedious task. This is due to the huge number of coefficients that arise while modelling the Earth's non-spherical gravity field. It is expected that DE can handle the trajectory optimization problem with the non-spherical gravity dynamical model.

List of symbols

DE	Differential evolution
TPBVP	Two-point boundary value problem
GTO	Geosynchronous transfer orbit
GSO	Geosynchronous orbit
CR	Crossover ratio
F	Mutation factor
NP	Population size
μ_p	Gravitational parameter of the] primary body (Earth)
μ_s	Gravitational parameter of the secondary body
r	Radial distance from the centre of the Earth
r_s	Radial distance from the centre of the secondary body
$\vec{\alpha}$	Acceleration vector due to thrust
m	Spacecraft mass
I_{sp}	Specific impulse
$\vec{\mathbf{x}}$	State vector
$\vec{\lambda}$	Costate vector
Φ_f	Terminal cost function
J_{time}	Time-optimal cost function
J_{fuel}	Fuel-optimal cost function
$\hat{h}$	Angular momentum unit vector
$\vec{\mathbf{e}}$	Eccentricity vector
T_{max}	Maximum available thrust
$\boldsymbol{H_{time}}$	Time-optimal Hamiltonian
$\boldsymbol{H_{fuel}}$	Fuel-optimal Hamiltonian
$\vec{\alpha}^*$	Optimal acceleration vector

References

[1] Gopinath N 2003 Optimal low thrust orbit transfer from GTO to geosynchronous orbit and stationkeeping using electric propulsion system. In: *Proceedings of the 54th International Astronautical Congress of the International Astronautical Federation, the International Academy of Astronautics, and the International Institute of Space Law*

[2] Falck R and Dankanich J 2012 Optimization of low-thrust spiral trajectories by collocation. In: *Proceedings of the AIAA/AAS Astrodynamics Specialist Conference*, p. 4423

[3] Falck R D, Sjauw W K and Smith D A 2014 Comparison of low-thrust control laws for applications in planetocentric space. In: *Proceedings of the 50th AIAA/ASME/SAE/ASEE Joint Propulsion Conference*, p. 3714

[4] Haberkorn T, Martinon P and Gergaud J 2004 Low thrust minimum-fuel orbital transfer: a homotopic approach. *J. Guidance Control Dyn.* 27(6): 1046–1060

[5] Kirk D E 2012 *Optimal control theory: an introduction*. Courier Corporation

[6] Nath P and Ramanan R V 2016 Precise halo orbit design and optimal transfer to halo orbits from earth using differential evolution. *Adv. Space Res.* 57(1): 202–217

[7] Storn R and Price K 1997 Differential evolution—a simple and efficient heuristic for global optimization over continuous spaces. *J. Glob. Optim.* 11(4): 341–359

[8] Fehlberg E 1968 *Classical fifth, sixth, seventh and eighth order Runge–Kutta formulas with stepsize control*. NTRS, NASA